Second Harmonic Generation Susceptibilities from Symmetry Adapted Wannier Functions

Bing-Hua Lei,[1,2] Shilie Pan,[1,2] Zhihua Yang,[1,2,*] Chao Cao,[3,1,†] and David J. Singh[4,5,‡]

[1]*CAS Key Laboratory of Functional Materials and Devices for Special Environments, Xinjiang Technical Institute of Physics and Chemistry, CAS, and Xinjiang Key Laboratory of Electronic Information Materials and Devices, 40-1 South Beijing Road, Urumqi 830011, China*

[2]*Center of Materials Science and Optoelectronics Engineering, University of Chinese Academy of Sciences, Beijing 100049, China*

[3]*Department of Physics, Condensed Matter Group, Hangzhou Normal University, Hangzhou 310036, China*

[4]*Department of Physics and Astronomy, University of Missouri, Columbia, Missouri 65211-7010, USA*

[5]*Department of Chemistry, University of Missouri, Columbia, Missouri 65211, USA*

(Received 11 October 2019; accepted 2 October 2020; published 30 October 2020)

Elucidating the orbital level origin of second harmonic generation (SHG) in materials and identifying the local contributions is a long-standing challenge. We report a first principles approach for the SHG where the contributions from individual orbitals or atoms can be evaluated via symmetry adapted Wannier functions without semiempirical parameters. We apply this method to the common SHG materials $KBe_2BO_3F_2$, $KCaCO_3F$, and β-BaB_2O_4, and show that the orbitals on noncentrosymmetric sublattices are responsible for SHG effect and the energies of these orbitals control the magnitude.

DOI: 10.1103/PhysRevLett.125.187402

Nonlinear optical (NLO) interactions between intense laser fields and condensed matter have been extensively studied since frequency doubling was observed in quartz [1]. Second harmonic generation (SHG) has emerged as the most practical and widely used approach for extending the solid-state laser spectrum to ultraviolet and deep-ultraviolet (UV) or infrared and far infrared regions [2–11]. Further, SHG can be applied in quantum up-conversion [12], driving polariton Fano resonances [13] and generating optical quantum mechanical superposition cat states [14]. These can enable production and manipulation of entangled photons for quantum information [15–20]. Since 1980, large size KH_2PO_4 single crystals have been grown. These provided a revolutionary breakthrough in overcoming the ultraviolet wall in all-solid-state lasers [21,22]. Subsequently, in 1985, β-BaB_2O_4 (β-BBO) [23] was reported to be a promising NLO crystal and was rapidly industrialized because it enables high-power UV and extends the UV spectrum. However, to date, no crystal can be used to generate high-power deep UV directly in industry. Although $KBe_2BO_3F_2$ (KBBF) [24–27] can produce deep UV directly, its platelike habit prevented growth of large-size single crystals, limiting applications. Discovery of new materials is critical.

Historically, calculation of SHG coefficients used band theory [28]. This suffers from a severe explicit divergence in the static limit. However, Aspnes proved that the divergent term vanishes for cubic crystals [29]. Ghahramani *et al.* then used a sum rule to obtain a general formalism free of divergence [30,31]. The methodology was further improved by systematic separation of inter- and intraband contributions [32]. Aversa and Sipe used the length gauge instead of the velocity gauge to give expressions avoiding unphysical divergences [33]. Subsequently, a general mixing frequency-dependent formalism was proposed [34] and the local field effect was also discussed [35–37]. Many approaches can be used to calculate the global SHG coefficients, including summation of states based on perturbation theory [30,31,38], Wannier and Bloch orbital-based methods [39], density-functional perturbation theory [40], and Berry phase methods [41–43]. However, obtaining global SHG coefficients is not sufficient for identifying and distinguishing underlying response mechanisms in terms of chemistry and structure. Identification of contributions from particular anionic groups or cations has been done by real-space cutting with semiempirical parameters [44,45]. The contribution of particular bonds can be evaluated by a localized-bond-charge model [46] based on bonding characteristics. What is lacking is a pure *ab initio* method for isolating SHG contributions at atomic or orbital levels. How this can be done has been an important open question.

Extended Bloch functions are widely used in SHG calculations. Physically, the SHG response [44] comes from virtual electron (VE) processes, virtual hole (VH) processes, and in early formulations also a two-band transition process, later shown to be exactly zero [38]. The static limit SHG coefficients are $\chi^{(2)}_{ijk} = \chi^{(2)}_{ijk}(\mathrm{VE}) + \chi^{(2)}_{ijk}(\mathrm{VH})$. The expressions are in terms of momentum matrices $p^i_{mn,\mathbf{k}} = \langle u_{m\mathbf{k}}|\hat{p}^i|u_{n\mathbf{k}}\rangle$ and energies $\epsilon_{m\mathbf{k}} = \langle u_{m\mathbf{k}}|\hat{H}|u_{m\mathbf{k}}\rangle$,

$$\chi^{(2)}_{ijk}(\mathrm{VE}) = \frac{e^3}{2\hbar^2 m^3}\sum_{vcc'}\int\frac{d\mathbf{k}^3}{4\pi^3}P(ijk)\mathrm{Im}[p^i_{vc}p^j_{cc'}p^k_{c'v}]\left(\frac{1}{\omega^3_{cv}\omega^2_{vc'}}+\frac{2}{\omega^4_{vc}\omega_{c'v}}\right), \tag{1}$$

$$\chi^{(2)}_{ijk}(\mathrm{VH}) = \frac{e^3}{2\hbar^2 m^3}\sum_{vv'c}\int\frac{d\mathbf{k}^3}{4\pi^3}P(ijk)\mathrm{Im}[p^i_{vv'}p^j_{v'c}p^k_{cv}]\left(\frac{1}{\omega^3_{cv}\omega^2_{v'c}}+\frac{2}{\omega^4_{vc}\omega_{cv'}}\right). \tag{2}$$

Here, i, j, and k are Cartesian components, and v/v' and c/c' are band indices for valence and conduction bands, respectively. The implicit $\mathbf{k}$ dependence of these indices is understood. $\omega_{mn,\mathbf{k}} = (\epsilon_{m\mathbf{k}} - \epsilon_{n\mathbf{k}})/\hbar$ is the energy difference between Bloch states of the mth and nth bands. $P(ijk)$ is the full permutation and explicitly shows the Kleinman symmetry. Calculated SHG coefficients by this approach generally agree well with experimental values when the density-functional theory (DFT) band gap is corrected by a scissors operator [47]. Bloch waves are extensive, leading to nonvanishing $p_{mn,\mathbf{k}}$ with arbitrary m and/or n. As a result, there is no simple physical way to define local contributions using this formula. However, according to phenomenological anionic group theory [48], which suggests that NLO effects are dominated by contributions from anionic groups, NLO effects should mainly be due to BO_3^{3-} in KBBF, $B_3O_6^{3-}$ in β-BBO, and CO_3^{2-} in $KCaCO_3F$ [49].

Wannier functions (WFs) provide an alternative. Although not strictly eigenfunctions of the Hamiltonian, they are well localized and can be used to study local physical properties, including electric polarization and orbital magnetization [50–52]. In addition, the Bloch sum of Wannier functions $|w_{\alpha\mathbf{k}}\rangle$ forms a natural local basis. This connects to the Bloch states $|u_{n\mathbf{k}}\rangle$ via a unitary transformation,

$$|w_{\alpha\mathbf{k}}\rangle = \sum_n U^{\mathbf{k}}_{n\alpha}|u_{n\mathbf{k}}\rangle. \tag{3}$$

The Wannier basis is further related with the local Wannier orbitals $|\mathbf{R}\alpha\rangle$ through

$$|\mathbf{R}\alpha\rangle = \frac{V}{(2\pi)^3}\int_{\mathrm{BZ}}\exp^{-i\mathbf{k}\cdot\mathbf{R}}|w_{\alpha\mathbf{k}}\rangle d\mathbf{k}^3. \tag{4}$$

Here, maximally projected WFs [53] were adopted so that crystal symmetry is retained. We can analyze local orbital contributions to the SHG using the local Wannier representation. To evaluate the contribution from a set of orbitals $\aleph$, we first project all valence states $|n\mathbf{k}\rangle \in \{v\}$ to the atomiclike Wannier orbital $|w_\alpha\rangle$ and get the projection coefficients $C^\alpha_{n\mathbf{k}}$

$$|n\mathbf{k}\rangle = \sum_\alpha C^\alpha_{n\mathbf{k}}|w_{\alpha\mathbf{k}}\rangle. \tag{5}$$

According to Eqs. (1) and (2), $\chi^{(2)}_{ijk}$ can be decomposed as the sum of contributions from different valence bands, $\chi^{(2)}_{ijk,n\mathbf{k}}$ ($|n\mathbf{k}\rangle \in \{v\}$). Therefore $|C^\alpha_{n\mathbf{k}}|^2$ is the weight of w_α to the nth valence band-decomposed SHG $\chi^{(2)}_{ijk,n\mathbf{k}}$. Then, the contributions to the total SHG $\chi^{(2)}_{ijk,w_\alpha}$ can be obtained using

$$\chi^{(2)}_{ijk,w_\alpha} = \sum_{|n\mathbf{k}\rangle\in\{v\}}|C^\alpha_{n\mathbf{k}}|^2\chi^{(2)}_{ijk,n\mathbf{k}}. \tag{6}$$

Additional details are in the Supplemental Material [54].

We take KBBF, β-BBO, and $KCaCO_3F$ as examples and apply this method to analyze the orbital contributions. These are representative of high-performance NLO borates with BO_3^{3-} or $B_3O_6^{3-}$ groups, carbonates with CO_3^{2-} groups, which crystallize in the space groups $R32$, $R3c$, and $P\bar{6}2m$, respectively. The crystal structures of KBBF [24], $KCaCO_3F$ [49], and β-BBO [23] and the definitions of the local orbital directions are shown in Fig. S1 [54]. Table S1 gives experimental and DFT lattice constants and atom positions.

Interpolated Wannier and DFT [55] band structures are compared in Fig. 1. For clarity, high symmetry lines and states between $E_F - 10$ and $E_F + 10$ eV are shown, with Fermi level E_F at the middle of gap. Full band structures and wider energy ranges are in Fig. S2 [54]. The DFT band gaps without scissors corrections are 6.06, 4.35, and 4.82 eV. A scissors operator [47] including the Ward identity correction for the momentum operator [59] was

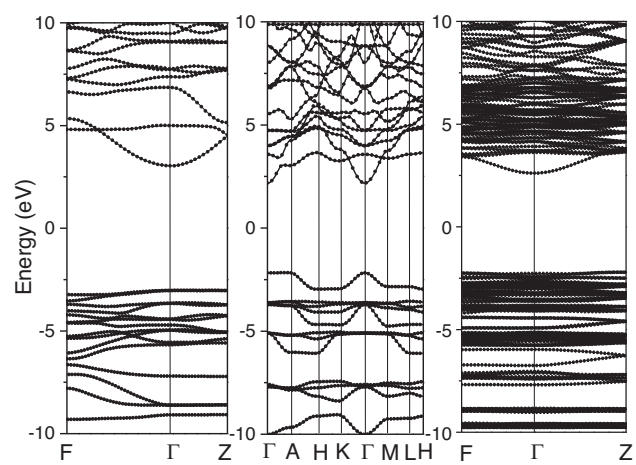

FIG. 1. Band structures of KBBF, $KCaCO_3F$, and β-BBO. Solid lines: DFT bands; dots: Wannier-interpolated bands.

TABLE I. Calculated (Cal.) static nonlinear susceptibilities (pm/V) as well as experimental (Expt.) values for KBBF, $KCaCO_3F$, and β-BBO and contributions (Con., pm/V) of atomic orbitals to the largest SHG coefficient[a].

Material		Orbital	Contributions	Orbital	Contributions
KBBF		K p	0.00	O sp^2-3	0.00
Calculated	Experimental	F sp^2 1, 2, 3	0.04	O $2p_z$	0.33
$d_{11} = 0.49$	$d_{11} = 0.47$	F $2p_z$	0.00	Sum	0.49
$d_{14} = -0.02$	$d_{14} < 0.01$	O sp^2 1, 2	0.02		
$KCaCO_3F$		K p	0.00	O sp^2 1,2	0.26
Calculated	Experimental	Ca p	−0.02	O sp^2 3	0.00
$d_{22} = 1.16$	$d_{22} \approx 1.40$	F sp^2 1, 2, 3	0.02	O $2p_z$	0.60
		F $2p_z$	0.00	Sum	1.16
β-BBO		Ba $5s$	0.01	O^t sp^2 1,2	0.48
Calculated	Experimental	Ba $5p_{x,y,z}$	−0.07	O^t sp^2 3	0.02
$d_{11} = 1.69$	$d_{11} = 1.60$	O^b sp^2 1, 2	0.00	O^t $2p_z$	0.72
$d_{31} = 0.03$	$d_{31} = 0.11$	O^b sp^2 3	−0.02	Sum	1.69
$d_{33} = 0.00$	$d_{33} \approx 0.00$	O^b $2p_z$	0.21		

[a]O^t and O^b stand for terminal oxygen and bridge oxygen in B_3O_6 group. The sp^2 1, sp^2 2, sp^2 3 are $1/\sqrt{3}s1/\sqrt{6}px + 1/\sqrt{2}py$, $1/\sqrt{3}s1/\sqrt{6}px1/\sqrt{2}py$, and $1/\sqrt{3}s + 2/\sqrt{6}px$, respectively. Here, the x direction is the bonding direction between B-O or C-O atoms, and z direction is perpendicular to the BO_3^{3-} plane or CO_3^{2-} plane. sp^2 1, 2 or 1, 2, 3 are symmetry equivalent. Here we give the contribution of each orbital and the total contribution is the sum. Following convention, Voigt notation is used contracting the last two indices (11 = 1; 22 = 2; 33 = 3; 32, 23 = 4; 31, 13 = 5; 12, 21 = 6) [60] and $d = \chi^{(2)}/2$.

applied with the experimental gaps of 8.43, 6.22, and 6.52 eV for KBBF, $KCaCO_3F$, and β-BBO, respectively. Then the calculated SHG coefficients are comparable with experimental values (Table I).

Table I also gives calculated orbital contributions to the SHG. The orbital contribution weight is defined as $W(\alpha) = \chi^{(2)}_{ijk,w_\alpha}/\chi^{(2)}_{ijk}$. The total weights of the oxygen sp^2 (see footnote of Table I for definitions) and $2p_z$ orbitals for KBBF, β-BBO, and $KCaCO_3F$ are 0.76, 0.96, and approximately 1.00, respectively. The fact that oxygen sp^2 or p_z orbitals have the largest contribution to the SHG is in accord with anionic group theory. In all three materials, the nonbonding oxygen orbital (O p_z orbital) contributes considerably to the SHG (from ~52% to ~68%), whereas σ bonds (O sp^2 3) between oxygen and boron or carbon in the planes of the BO_3/CO_3 groups make negligible contribution (1%–1%). However, contributions from O sp^2 1 or O sp^2 2 orbitals vary among the materials. In KBBF, the σ bonds (O sp^2 1 or O sp^2 2) between oxygen and beryllium have almost no contribution. However, in $KCaCO_3F$, these two orbitals are the ionic bonds between oxygen and cations and play an important role in SHG response (22% each). In β-BBO, there are two types of oxygen atoms, namely the bridge oxygen and the terminal oxygen (Fig. 2). The contributions from σ bonds (O sp^2 1 or O sp^2 2 orbitals) of bridge oxygens, are zero, whereas the ionic bonds (O sp^2 1 or O sp^2 2 orbitals) of the terminal oxygen contribute 56% of the SHG.

The orbital contributions can be understood by considering the symmetry and the orbital energies. The SHG coefficient $\chi^{(2)}_{ijk}$ is an antisymmetric tensor with three indices, each representing a certain direction. Therefore, in centrosymmetric crystals, the SHG coefficients are zero. In noncentrosymmetric crystals, the crystal structure in general can be decomposed to centrosymmetric and noncentrosymmetric sublattices. On one hand, the orbitals on centrosymmetric sublattices have no contribution to SHG coefficients by themselves. However, since the Wannier orbitals on centrosymmetric sublattices also have noncentrosymmetric content due to the construction, they generally have noncentrosymmetric tails (Fig. S3) [54]. Therefore, the contribution from orbitals on centrosymmetric sublattices is very small but not zero. On the other hand, $\chi^{(2)}_{ijk}$ decays as fast as ω^{-5}, according to Eqs. (1)

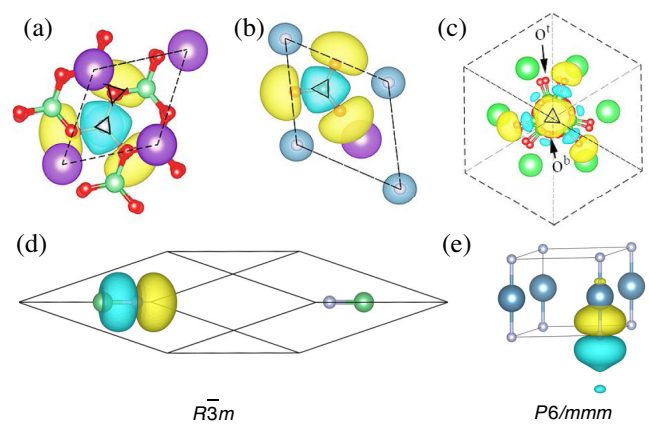

FIG. 2. sp^2-3-like Wannier orbitals of oxygens (red) in (a) KBBF, (b) $KCaCO_3F$, and (c) some terminal oxygens of β-BBO. The triangles represent C_3 symmetries and the triangle with horns in (a) represent that there is a 3_1 screw axis. The sublattice with $R\bar{3}m$ or $P6/mmm$ symmetries consisting of only F (gray) and Be (gray green) in (d) KBBF, as well as F and Ca (gray blue) in (e) $KCaCO_3F$. The colors of remaining atoms are B (green), C (black), K (purple), Ba (bright green).

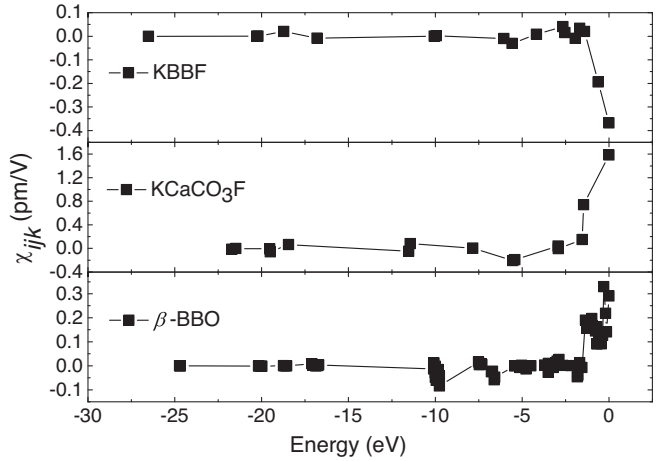

FIG. 3. Contribution to the SHG coefficients of Bloch states of KBBF, $KCaCO_3F$, and β-BBO. Here energy is relative to the band edge.

and (2), where ω is at least the size of the band gap. Therefore, the contribution from orbitals on noncentrosymmetric sublattices would be substantially affected by their energy levels, and contributions from deep-energy bands will be small.

Figure 3 shows the contribution of Bloch states to SHG coefficients in energy space. We use the Bloch states at Γ as an illustration. The calculated SHG coefficients d_{11} for KBBF, d_{22} for $KCaCO_3F$, and d_{11} for β-BBO on Γ are 0.50, 1.40, and 1.60 pm/V. These values are consistent with experimental values as well as results using dense k-point meshes (Table I). As seen in Fig. 3, only states near the Fermi level give large contributions and Bloch states below -2.5 eV, relative to the valence band top, contribute little. For a given crystal structure, the orbitals can be projected on a set of symmetrically equivalent orbitals (Figs. S4–S6) [54]. Thus, the contribution of these symmetrically equivalent orbitals is

$$\chi^{(2)}_{\aleph} = \sum_{\alpha,n} \langle w_\alpha | v_n \rangle \chi^{(2)}_{ijk,v_n} \langle v_n | w_\alpha \rangle. \tag{7}$$

The materials we investigated generally have C_3 symmetry. For the oxygen p_z-like orbitals, there are three equivalent O p_z orbitals located on symmetrically equivalent sites, and $\hat{T}_{C_3}\chi^{(2)}_{111}\hat{T}^{-1}_{C_3} = \chi^{(2)}_{111}$ for KBBF and β-BBO or $\hat{T}_{C_3}\chi^{(2)}_{222}\hat{T}^{-1}_{C_3} = \chi^{(2)}_{222}$ for $KCaCO_3F$. Therefore, their total contribution amounts up to $3\sum_n \langle p_z | v_n \rangle \chi^{(2)}_{111,v_n} \langle v_n | p_z \rangle$ or $3\sum_n \langle p_z | v_n \rangle \chi^{(2)}_{222,v_n} \langle v_n | p_z \rangle$. In addition, O p_z orbitals in these three compounds have large weight in bands near the band edges (Fig. S7) [54]. As a result, the set of p_z-like orbitals makes a large contribution to SHG in all cases studied. Similar arguments can always be applied to planar chemical groups containing symmetrically equivalent atoms, and therefore planar groups such as BO_3^{3-}, $B_3O_6^{3-}$, and CO_3^{2-} always play a important role in SHG response. Therefore, as seen in Table I, all O p_z-like orbitals [Figs. S4(d), S5(d), and S6] [54] make major contributions in these materials due to the superposition of p_z orbitals. In contrary, the F p_z-like orbitals in KBBF and $KCaCO_3F$, which connected fluorine to beryllium or calcium, are located on a centrosymmetric sublattice. As shown in Fig. 2(d), beryllium and fluorine occupy Wyckoff position c so that the sublattice has an inversion center at the center of the unit cell and the space group is $R\bar{3}m$. Similarly, in $KCaCO_3F$ [Fig. 2(e)], an inversion center can also be found for the calcium and fluorine sublattices with a space group of $P6/mmm$ (Wyckoff positions b and a) at the center of the unit cell. The detailed Wyckoff positions in crystals are in Table S1 [54]. Although the F p_z orbitals are significant in the Bloch states near the band edge in KBBF (Fig. S7) [54], their contribution to SHG coefficients is limited due to the restriction of sublattice symmetry. This is seen in the results (Table I).

Now, we analyze the sp^2-like orbitals of oxygen in Fig. 2. The sp^2-like orbitals are bonding states between X ($X = \mathrm{C}$, B) atoms and oxygens. The three symmetrical equivalent Wannier orbitals are $|w_1\rangle = |X\,sp^2\,1\rangle - |\mathrm{O}\,sp^2 1\rangle$, $|w_2\rangle = |X\,sp^2 2\rangle - |\mathrm{O}\,sp^2 2\rangle$, and $|w_3\rangle = |Xsp^2 3\rangle - |\mathrm{O}\,sp^2\,3\rangle$. In KBBF or β-BBO, these sp^2 orbitals occupy deep energies (below $\sim$3 eV relative to the top of valence bands) far from the band edge (Fig. S7) and the density of states (DOS) (Fig. S8) [54]. Therefore, the sp^2 3, the bonding sp^2-1-, and the sp^2-2-like Wannier orbitals of oxygens in KBBF and the bridge oxygen in β-BBO make little contribution. In comparison, in $KCaCO_3F$, the sp^2-1- and the sp^2-2-like orbitals are not bonded with the central atom but weakly hybridize with d orbitals from surrounding cations (Fig. S8) [54]. Thus, these orbitals have large weight near the band edge. They will therefore make significant contributions to SHG coefficients, consistent with Table I.

To further elaborate our argument, we constructed a $CaCO_3$ crystal cell with a CO_3 and three calcium atoms along the rotation axis, as shown in Fig. 4(a). In this case, the sp^2-1- and sp^2-2-like orbitals do not hybridize with cations due to the symmetry restriction. We use the same method to analyze the contributions to the SHG. The result shows that the SHG coefficient d_{11} is reduced to 0.50 pm/V and mainly comes from the p_z-like orbitals. The contribution from the rest of the orbitals is negligible. The Wannier orbitals including sp^2 1 and sp^2 2 of $KCaCO_3F$ and artificial $CaCO_3$ are shown in Figs. 4(b) and 4(c).

In β-BBO, three BO_3^{3-} groups trimerize into a $B_3O_6^{3-}$ group by sharing three oxygens. Therefore, the oxygen atoms can be classified as bridge oxygens (O^b) that bond with two boron atoms and terminal oxygens (O^t) that bond only one boron, as shown in Fig. 2. The sp^2-1- and sp^2-2-like orbitals for terminal oxygens have sizable contributions because of the hybridization between oxygen and

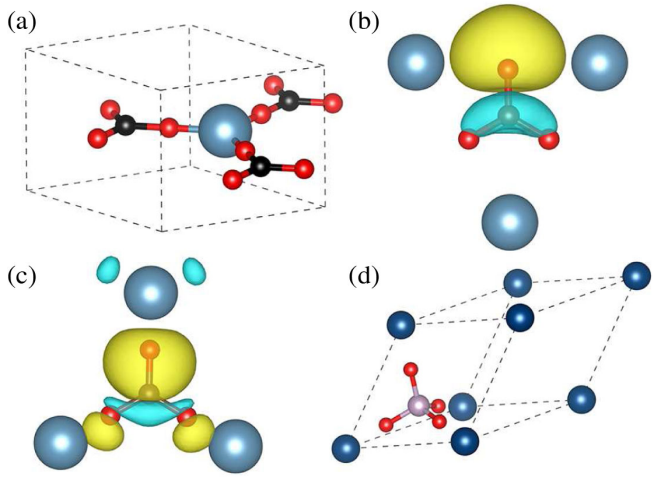

FIG. 4. Artificial crystal structures of (a) $CaCO_3$, as well as (d) $AlPO_4$ and the sp^2-1- as well as sp^2-2-like orbitals in (b) $CaCO_3F$ and (c) artificial $CaCO_3$. Dark blue and pink represent aluminum and phosphorus, respectively.

strontium. Therefore, under the C_3 symmetry, the contributions of p_z-like orbitals have large weight in bands near the band edge so that they always make large contributions to the SHG. In addition, although the barium atoms in β-BBO are in a noncentrosymmetric sublattice ($R3$), these orbitals do not contribute near the band edge (Fig. S8) [54], so they have little SHG contribution.

Our argument is not limited to planar groups with C_3 symmetry. It can also be applied to other groups subjected to other symmetries. To verify this, we constructed a crystal $AlPO_4$, with a face-centered-cubic lattice. The Al and P are at (0.00, 0.00, 0.00) and (0.25, 0.25, 0.25), while oxygen is along the line between these atoms. The crystal structure is shown in Fig. 4(d). In this case, the P—O bonds or s orbitals have very little contribution because they appear at high binding energy. The remaining nonbonding oxygen orbitals do not hybridize with other atoms. The oxygen atoms classified by mirror symmetry are shown in Fig. S9(c) [54]. Also, the oxygen sublattice is centrosymmetric. Therefore, the SHG is expected to be very small. As anticipated, the result of direct calculations is only 0.02 pm/V. To further verify this idea, we rotated the PO_4 tetrahedral to break the inversion symmetry of oxygen sublattice [Figs. S9(b) and S9(d)] [54]. The calculated SHG coefficient is substantially enhanced to 0.61 pm/V, whereas the band gap changes very little (from 4.45 to 4.48 eV). This $AlPO_4$ compound is isostructural to BPO_4 [61], which has the largest SHG of compounds built of tetrahedra with deep ultraviolet cutoff edges. Therefore, the lack of inversion in oxygen sublattice, whose p orbitals dominate the DOS near the valence band maximum, is crucial for strong SHG response.

In conclusion, we used symmetrized Wannier functions to identify the underlying mechanism of SHG response in NLO materials. The orbital contributions to the SHG are dictated by the symmetry of the sublattice and controlled by their energies. More specifically, only orbitals forming noncentrosymmetric sublattices and occurring in the top valence bands make substantial contributions to the SHG coefficient. The analysis is based on symmetry considerations, applicable to NLO materials in general, and may be helpful in identifying new NLO materials with large SHG effect.

This work was supported by the National Natural Science Foundation of China (Grants No. 51922014, No. 11774414, No. 11274006, No. 11874137), the Key Research Program of Frontier Sciences, CAS (ZDBS-LY-SLH035), and the Xinjiang Program of Introducing High-Level Talents.

*zhyang@ms.xjb.ac.cn
†ccao@hznu.edu.cn
‡singhdj@missouri.edu

[1] P. A. Franken, A. E. Hill, C. W. Peters, and G. Weinreich, Phys. Rev. Lett. **7**, 118 (1961).
[2] C. Ding, J. R. W. Ulcickas, F. Deng, and G. J. Simpson, Phys. Rev. Lett. **119**, 193901 (2017).
[3] K. Rojan, Y. Léger, G. Morigi, M. Richard, and A. Minguzzi, Phys. Rev. Lett. **119**, 127401 (2017).
[4] C. R. McDonald, K. S. Amin, S. Aalmalki, and T. Brabec, Phys. Rev. Lett. **119**, 183902 (2017).
[5] G. Vampa, C. R. McDonald, G. Orlando, D. D. Klug, P. B. Corkum, and T. Brabec, Phys. Rev. Lett. **113**, 073901 (2014).
[6] S. Ghimire, A. D. DiChiara, E. Sistrunk, P. Agostini, L. F. DiMauro, and D. A. Reis, Nat. Phys. **7**, 138 (2011).
[7] D. Cyranoski, Nature (London) **457**, 953 (2009).
[8] C. T. Chen, G. L. Wang, X. Y. Wang, and Z. Y. Xu, Appl. Phys. B **97**, 9 (2009).
[9] A. Cammarata and J. M. Rondinelli, ACS Photonics **1**, 96 (2014).
[10] X. Jiang, S. Luo, L. Kang, P. Gong, H. Huang, S. Wang, Z. Lin, and C. Chen, ACS Photonics **2**, 1183 (2015).
[11] B.-W. Liu, H.-Y. Zeng, X.-M. Jiang, G.-E. Wang, S.-F. Li, L. Xu, and G.-C. Guo, Chem. Sci. **7**, 6273 (2016).
[12] C. E. Vollmer, C. Baune, A. Samblowski, T. Eberle, V. Handchen, J. Fiurasek, and R. Schnabel, Phys. Rev. Lett. **112**, 073602 (2014).
[13] Y. Wang, L. Liao, T. Hu, S. Luo, L. Wu, J. Wang, Z. Zhang, W. Xie, L. Sun, A. V. Kavokin, X. Shen, and Z. Chen, Phys. Rev. Lett. **118**, 063602 (2017).
[14] Y. Shen, S. M. Assad, N. B. Grosse, X. Y. Li, M. D. Reid, and P. K. Lam, Phys. Rev. Lett. **114**, 100403 (2015).
[15] H. Jin, P. Xu, X. W. Luo, H. Y. Leng, Y. X. Gong, W. J. Yu, M. L. Zhong, G. Zhao, and S. N. Zhu, Phys. Rev. Lett. **111**, 023603 (2013).
[16] H. Y. Leng, X. Q. Yu, Y. X. Gong, P. Xu, Z. D. Xie, H. Jin, C. Zhang, and S. N. Zhu, Nat. Commun. **2**, 429 (2011).
[17] H. Jin, F. M. Liu, P. Xu, J. L. Xia, M. L. Zhong, Y. Yuan, J. W. Zhou, Y. X. Gong, W. Wang, and S. N. Zhu, Phys. Rev. Lett. **113**, 103601 (2014).

[18] X.-C. Yao, T.-X. Wang, P. Xu, H. Lu, G.-S. Pan, X.-H. Bao, C.-Z. Peng, C.-Y. Lu, Y.-A. Chen, and J.-W. Pan, Nat. Photonics **6**, 225 (2012).

[19] X.-L. Wang, L.-K. Chen, W. Li, H.-L. Huang, C. Liu, C. Chen, Y.-H. Luo, Z.-E. Su, D. Wu, Z.-D. Li, H. Lu, Y. Hu, X. Jiang, C.-Z. Peng, L. Li, N.-L. Liu, Y.-A. Chen, C.-Y. Lu, and J.-W. Pan, Phys. Rev. Lett. **117**, 210502 (2016).

[20] X.-L. Wang, Y.-H. Luo, H.-L. Huang, M.-C. Chen, Z.-E. Su, C. Liu, C. Chen, W. Li, Y.-Q. Fang, X. Jiang, J. Zhang, L. Li, N.-L. Liu, C.-Y. Lu, and J.-W. Pan, Phys. Rev. Lett. **120**, 260502 (2018).

[21] C. Belouet, Prog. Cryst. Growth Charact. **3**, 121 (1980).

[22] J. J. D. Yoreo, A. K. Burnham, and P. K. Whitman, Int. Mater. Rev. **47**, 113 (2002).

[23] C. Chen, A. Jiang, and G. You, Sci. Sin. Ser. B **28**, 235 (1985).

[24] L. Mei, X. Huang, Y. Wang, Q. Wu, B. Wu, and C. Chen, Z. Kristallogr. Cryst. Mater. **210**, 93 (1995).

[25] C. Chen, Z. Y. Xu, D. Q. Deng, J. Zhang, G. K. L. Wong, B. C. Wu, N. Ye, and D. Y. Tang, Appl. Phys. Lett. **68**, 2930 (1996).

[26] C. Chen, N. Ye, J. Lin, J. Jiang, W. Zeng, and B. Wu, Adv. Mater. **11**, 1071 (1999).

[27] C. Chen, Y. Wang, Y. Xia, B. Wu, D. Tang, K. Wu, Z. Wenrong, L. Yu, and L. Mei, J. Appl. Phys. **77**, 2268 (1995).

[28] P. N. Butcher and T. P. McLean, Proc. Phys. Soc. **81**, 219 (1963).

[29] D. E. Aspnes, Phys. Rev. B **6**, 4648 (1972).

[30] E. Ghahramani, D. J. Moss, and J. E. Sipe, Phys. Rev. B **43**, 8990 (1991).

[31] E. Ghahramani, D. J. Moss, and J. E. Sipe, Phys. Rev. Lett. **64**, 2815 (1990).

[32] J. E. Sipe and E. Ghahramani, Phys. Rev. B **48**, 11705 (1993).

[33] C. Aversa and J. E. Sipe, Phys. Rev. B **52**, 14636 (1995).

[34] J. E. Sipe and A. I. Shkrebtii, Phys. Rev. B **61**, 5337 (2000).

[35] Z. H. Levine, Phys. Rev. B **42**, 3567 (1990).

[36] Z. H. Levine and D. C. Allan, Phys. Rev. B **44**, 12781 (1991).

[37] J. Chen, L. Jönsson, J. W. Wilkins, and Z. H. Levine, Phys. Rev. B **56**, 1787 (1997).

[38] B. Zhang, M.-H. Lee, Z. Yang, Q. Jing, S. Pan, M. Zhang, H. Wu, X. Su, and C.-S. Li, Appl. Phys. Lett. **106**, 031906 (2015).

[39] A. Dal Corso and F. Mauri, Phys. Rev. B **50**, 5756 (1994).

[40] M. Veithen, X. Gonze, and P. Ghosez, Phys. Rev. B **71**, 125107 (2005).

[41] D. Xiao, M.-C. Chang, and Q. Niu, Rev. Mod. Phys. **82**, 1959 (2010).

[42] R. D. King-Smith and D. Vanderbilt, Phys. Rev. B **47**, 1651 (1993).

[43] D. Vanderbilt and R. D. King-Smith, Phys. Rev. B **48**, 4442 (1993).

[44] J. Lin, M.-H. Lee, Z.-P. Liu, C. Chen, and C. J. Pickard, Phys. Rev. B **60**, 13380 (1999).

[45] C.-G. Duan, J. Li, Z.-Q. Gu, and D.-S. Wang, Phys. Rev. B **59**, 369 (1999).

[46] B. F. Levine, Phys. Rev. B **7**, 2600 (1973).

[47] J. L. P. Hughes and J. E. Sipe, Phys. Rev. B **53**, 10751 (1996).

[48] C. Chen, Y. Wu, and R. Li, Int. Rev. Phys. Chem. **8**, 65 (1989).

[49] G. Zou, N. Ye, L. Huang, and X. Lin, J. Am. Chem. Soc. **133**, 20001 (2011).

[50] N. Marzari and D. Vanderbilt, Phys. Rev. B **56**, 12847 (1997).

[51] I. Souza, N. Marzari, and D. Vanderbilt, Phys. Rev. B **65**, 035109 (2001).

[52] N. Marzari, A. A. Mostofi, J. R. Yates, I. Souza, and D. Vanderbilt, Rev. Mod. Phys. **84**, 1419 (2012).

[53] V. I. Anisimov, D. E. Kondakov, A. V. Kozhevnikov, I. A. Nekrasov, Z. V. Pchelkina, J. W. Allen, S.-K. Mo, H.-D. Kim, P. Metcalf, S. Suga, A. Sekiyama, G. Keller, I. Leonov, X. Ren, and D. Vollhardt, Phys. Rev. B **71**, 125119 (2005).

[54] See Supplemental Material at http://link.aps.org/supplemental/10.1103/PhysRevLett.125.187402 for details of the derivation, crystal structures, and orientations of the orbitals, as well as first principles and Wannier band structures.

[55] All calculations were done with the projector augmented wave method in the Vienna *ab initio* Simulation Package (VASP) [56–58]. The plane wave energy cutoff was 480 eV. The Brillouin zone samplings were done with $8 \times 8 \times 8$, $8 \times 8 \times 8$, and $6 \times 6 \times 6$ meshes for KBBF, $KCaCO_3F$, and β-BBO, respectively. Crystal structures were optimized by energy minimization. The convergence criterion for this optimization was that the residual atomic forces are less than 0.01 eV/Å, and the total pressure is smaller than 0.5 kB.

[56] P. E. Blochl, Phys. Rev. B **50**, 17953 (1994).

[57] G. Kresse and J. Hafner, Phys. Rev. B **47**, 558 (1993).

[58] G. Kresse and D. Joubert, Phys. Rev. B **59**, 1758 (1999).

[59] Z. H. Levine and D. C. Allan, Phys. Rev. Lett. **63**, 1719 (1989).

[60] R. W. Boyd, *Nonlinear Optics* (Elsevier, New York, 2003).

[61] X. Zhang, L. Wang, S. Zhang, G. Wang, S. Zhao, Y. Zhu, Y. Wu, and C. Chen, J. Opt. Soc. Am. B **28**, 2236 (2011).